NUMERICAL ANALYSIS OF DEBRIS-FLOW INTERACTION WITH OPEN BARRIERS

MADDALENA MARCHELLI[1], ALESSANDRO LEONARDI[2] AND MARINA PIRULLI[1]

[1] Polytechnic University of Turin
Corso Duca degli Abruzzi, 24 - 10129 Torino, Italy
maddalena.marchelli@polito.it - marina.pirulli@polito.it

[2] Idrostudi Srl
Area Science Park, Loc. Padriciano 99, 34149 Trieste, Italy
alessandro.leonardi.ing@gmail.com

Key words: Granular Materials, DEM, Debris Flow, Barrier, Slit Dam

Abstract. Debris flows are fast gravity-driven flows consisting of multiple interacting phases. Due to their rapid movement and destructive power, structural mitigation measures have become essential in order to prevent extensive damage to property and life. Among these structures, rigid barriers constitute an efficient system of mitigation, which induces sediment deposition in case of an event. The optimal design of these structures requires the impact force estimation, which has recently become a crucial issue. Because of this, numerous experimental and numerical investigations have been carried out in recent years concerning debris flow and their impact energy on rigid closed barriers [1]. However, there is a lack of information in the framework of rigid open barriers, especially for what concerns the influence of the outlet geometry. In this regard, many studies have examined the jamming of a single-outlet silo [2], where the mass discharges in the direction of gravity, but the jamming of particles on an inclined slope has not been sufficiently investigated yet. The present numerical study investigates the formation of arching behind an open barrier that partially arrests the flow of particles on an inclined channel. The nature of jamming, and the impact energy on the barrier are examined using DEM simulations for a fixed discharged mass, using different outlet sizes and inclines. The applied model is an improvement of the LBM-DEM code developed by Leonardi et al. [3]. Static friction is implemented with the spring-dashpot linear model and a directional constant torque model is included in order to describe rolling resistance due to elastic deformation and the effect of non-spherical particle shape. The resulting force and momentum at the flow base are analysed in detail together with the kinetic energy and the distribution of particles in the slit. The dynamic impact of the solid component alone is analysed in order to rationalize the design of open barriers. Indeed numerical examples show that a single

outlet could jam with a probability that decreases with the slope and the outlet size, but two adjacent outlets do not necessarily jam in the same configuration.

1   INTRODUCTION

Much research in recent years focuses on debris flow, recognizing it as one of the most devastating landslide phenomenon, in terms of loss of life and damage to structures and infrastructures. Debris flows are a mixture of water and non-plastic coarse material that flow in a steep channel [4]. Their destructive potential is due to the absence of premonitory signs, the extremely high velocity $(0.05 - 20$ m/s), the erosive capability and the long travel distance even on gentle slopes. In this perspective, the design of mitigation structures as countermeasures has become of great interest. Among these structures, the present study focuses on open rigid barriers, which constitute as efficient system for reducing kinetic energy, trapping sediment, and causing material deposition. Recently, more and more numerical and experimental investigations have been carried out in the frame of studying debris flow impact on rigid closed barrier [5, 1, 6]. Nevertheless, insufficient informations are available on open rigid barriers. In particular the influence of the outlet size on the trapping efficiency remains almost unstudied [7]. In this regard, many studies have examined the jamming of a single-outlet silo [8, 9, 2, 10, 11, 12], or a granular pile [13, 14], where the mass discharges in the direction of gravity. In those cases the granular material can generate bridges or arches, i.e. stable collective structures comprising several grains which can sustain the weight above them [15]. Arches can cause granular jamming in a fixed configuration that is mechanically stable, which results in a temporary or permanent clogging of the outlets of a barrier thus trapping the material behind it. Notwithstanding its importance for the retainment mechanism, the jamming of particles, and the formation of arches behind barriers built along an inclined plane, have not been sufficiently investigated yet.

The purpose of this work is to study arch formation behind a barrier, which in turn is a key factor for determining its trapping capability, and the impact energy exerted on the barrier itself. To achieve such goals, simulations are performed using a DEM model, using a fixed discharging mass treated as an assembly of rigid spheres with deformable contacts.

Real debris flows have a complex multi-phase nature, where sediments are mixed with an ambient fluid [4]. A complete description of this is outside of the scope this paper, which instead focuses on the different role played by the barrier outlet size and the slope inclination. The model is an improvement of the LBM-DEM code developed by Leonardi et al. [3], and a new and more sophisticated friction model is tested. Static friction is implemented with the spring-dashpot linear model and a directional torque model is included to consider both elastic deformation effect and non-spherical particle shape. This paper is organized as follows. A brief description of the model applied is introduced

in Sect. 2. In this section, constitutive parameters, initial condition and geometry of the analyses are specified. In Sect. 3 the main features of numerical results are illustrated. In Sect. 4 the role played by the variables and the outcomes are discussed. Finally in Sect. 5. conclusions and future perspectives on multiple outlets barrier are proposed.

2 THE DEM APPROACH AND SIMULATIONS

2.1 The DEM approach

Numerical simulations have been performed by employing the LBM-DEM code developed by Leonardi et al. [3]. This code has been improved by introducing rolling and static sliding friction, i.e. the resisting forces to sliding motion between two surface in contact. In the DEM model framework these forces arise when a particle-particle or particle-wall collision occurs. The linear dashpot model idealizes the contact as a parallel connection with a spring of stiffness k and a damper with viscous coefficient α. The tangential force $\mathbf{F^T}$ is capped by the normal force $\mathbf{F^N}$ through Coulomb's law $|\mathbf{F^T}| \leq \mu_s \mathbf{F^N}$. For the sliding case the dynamic friction is $\mathbf{F^T} = \mu_d \mathbf{F^N}$. The static ($\mu_s$) and the dynamic ($\mu_d$) friction coefficients follow the relation $\mu_d \leq \mu_s$. In DEM simulations the static situation requires an elastic spring to allow a restoring force, i.e. a non-zero remaining tangential force in static equilibrium due to the activated Coulomb friction. This spring represents the distance between the first contact point between two particles and the actual contact point, and is active as long as a contact is present. The model implemented in the code follows the solution proposed by Luding [16].

The present DEM model has been expanded by including a rolling resistance model, which consider the elastic and plastic contact deformation of the material and the effect of non-spherical shapes. In fact, the contact between two particles creates a deformation of the two bodies, whose contact forces no longer act on a single point, but over an area. Furthermore, a sort of rolling resistance arises also from the effect of a non-spherical particle shape. The employed DEM uses simple spheres to represent a real granular material, thus requiring a rolling resistance to take non-sphericity into account. A directional constant torque model has been adopted: a constant torque is applied, always contrasting the relative rotation between the two contacting bodies. The torque $\mathbf{M^R}$ is applied to each pair of particles in contact [17], as follows.

$$\mathbf{M}_i^R = -\mu_r F^N \frac{\boldsymbol{\omega}_{\text{rel}}}{|\boldsymbol{\omega}_{\text{rel}}|} A_r \tag{1}$$

$$\mathbf{M}_j^R = +\mu_r F^N \frac{\boldsymbol{\omega}_{\text{rel}}}{|\boldsymbol{\omega}_{\text{rel}}|} A_r \tag{2}$$

where i, j denote two generic particles, F^N is the modulus of the normal component of the particle-particle force, $\boldsymbol{\omega}_{\text{rel}} = \boldsymbol{\omega}_i - \boldsymbol{\omega}_j$ is the relative angular velocity, $A_r = (r_i r_j)/(r_i + r_j)$ the rolling radius, r the particle radius, and μ_r the rolling friction coefficient. This parameter is dimensionless, and is only a function of shape, material roughness, and of the rolling speed.

Following the approach proposed for implementing sliding and rolling resistance, a simple linear contact model, characterized by a normal and a tangential stiffness (k_N and k_S respectively) is chosen for the following simulations.

2.2 Simulations

The model geometry is illustrated in Fig. 1, where both the granular mass and the single-outlet rigid barrier are shown. The model is confined within a cubic domain, enclosed by walls with their own friction coefficient. The flow width is equal to 18 times
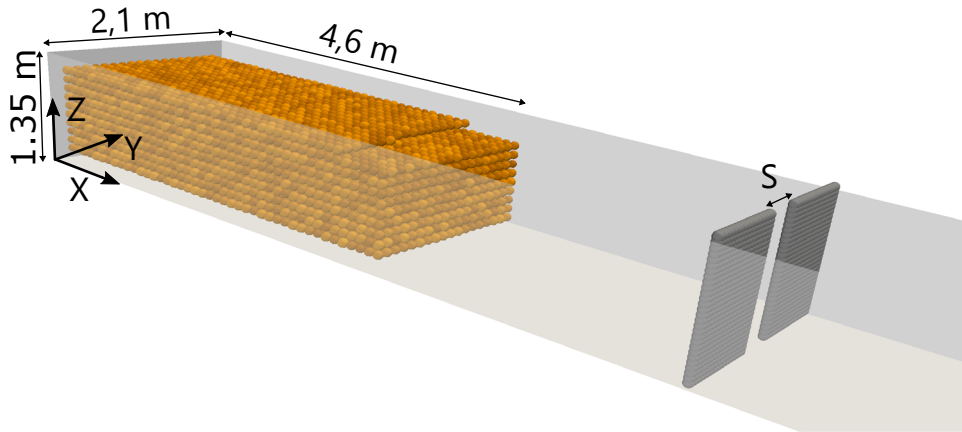
Figure 1: DEM Model, initial condition of the monodisperse spherical discharged mass and position of the barrier.

the average grain diameter D, so that the influence of the lateral boundary is minimized. The barrier width spans the whole transversal size of the domain, except for the outlet, positioned in the center of the barrier, and its height is equal to the domain height. For the sake of simplicity, the simulations consider a monodisperse granular flow modeled using rigid spherical grains. The geometrical characteristics as well as the constitutive parameters are reported in Table 1.

The initial velocity for the granular mass is set to zero, and the flow is driven by gravity. The obstacle is orthogonal to the sliding plane. Four different slopes θ are considered: $10°, 20°, 30°, 35°, 40°$, with the purpose of simulating inclinations smaller or greater than the internal friction angle ϕ_i, equal to $30°$, a typical value for soils. The wall-particle and the barrier-particle friction coefficients are here equal.

Generally, rigid open barrier are built in the fan apex area, where the slope is much lower than $30°$. However debris flow events are characterized also by the presence of water, which reduces the internal friction angle and increases mass mobility. In this view, the choice of simulating an inertial flow, in which frictional forces do not contrast and halt the motion, is essential in order to correctly estimate the trapping efficiency. Generally it is assumed that if $\theta \leq \phi_i$ the flow regime is frictional, while if $\theta \leq \phi_i$ it is mainly inertial. Furthermore, finding multiple barrier is not unusual, and is often required to

Table 1: Parameters considered in the numerical model. For the description of all parameters not defined here please refer to [3]

Number of particles	7640
Diameter D [m]	0.1
Density [kg/m^3]	2500
k_{N} [N/m]	10^6
k_{S} [N/m]	$\frac{2}{7}k_{\mathrm{N}}$
Restitution coefficient ζ [-]	0.2
$\mu_{\mathrm{s,particle\text{-}particle}}$, $\mu_{\mathrm{s,particle\text{-}wall}}$ [-]	0.577
$\mu_{\mathrm{r,particle\text{-}particle}}$ [-]	0.0678
$\mu_{\mathrm{r,particle\text{-}wall}}$ [-]	$2\mu_{\mathrm{r,particle\text{-}particle}}$
Domain size (XYZ) [m]	$20.00 \times 2.10 \times 1.35$
Mass discharge size (XYZ) [m]	$4.60 \times 1.90 \times 1.00$
Position of the front(X) [m]	4.725
Position of the filter barrier (X)[m]	8.00

catch material from high-energy supercritical flows rather than allowing the free saltation of grains downstream [7].

In addition to the slope inclination, also the outlet size S, (written as a multiple of the characteristic radius of the grains r), is varied, with the purpose of finding a critical S/r ratio above which no clogging occurs. For $\theta = 10°$ and $\theta = 20°$, the investigated S/r varies from 2 to 10. For the whole range an arching effect is always observed. Critical S/r is instead investigated for slope angles greater than internal friction angles, simulating until $S/r \leq 9 - 10$, depending on the considered slope. The study of both inclinations and S/r is in the perspective that the grain-trapping efficiency depends on both outlet width and flow condition.

3 RESULTS

In the perspective of a proper design of open rigid barriers, jamming occurrence and characteristics, as well as the maximum impact forces, need to be investigated. The numerical simulations carried out are analyzed in this view and in this section the numerical results are presented in detail. The formation of arching is examined analyzing the following parameters for each incline: (1) the ratio between the height of the arch H_{arch} and the height of the barrier H_{bar} with respect to the time of arching t_{stop}, referring to the first arrival time t_0. (Figs.2, 3), (2) the fraction of the material that is not retained $\%_{nr}$ with respect to the outlet width of the barrier, after a complete stop of the discharging mass is occurred (Fig. 4) . To compute the height of the arch, the outlet height has been subdivided in ten intervals, within which, for all outlet width, the kinetic energy of particles $E_{\mathbf{K,p}}$ has been calculated. If $\sum_{\mathbf{interval}} E_{E,\mathbf{p}} < 10^{-5}$ the particles are considered

halted. Figs. 2,3 plot with markers the center of each interval, when the mass halts and only if there is any retained mass inside.

Considering each slope angle θ, it is observed that:

- $\theta = 10°$: frictional forces prevail and the discharging mass is halted before it impacts against the barrier. Permanent arching occurs for each outlet dimension, but with a height far lower than the barrier height. Clogging time with respect to the first impact time is very short, around $2 - 5$ s, reaching a maximum value of 24 s by increasing the outlet width (Fig. 2 (A));

- $\theta = 20°$: frictional forces prevails as for $\theta = 10°$. Arching occurs for all outlet sizes with a greater height, but is not always rapid. For $S/r = 6$ stable clogging occurs progressively in time and for $S/r > 7$ formation is rapid but only later in time and involving only few layers of grains, (Fig. 2 (B));
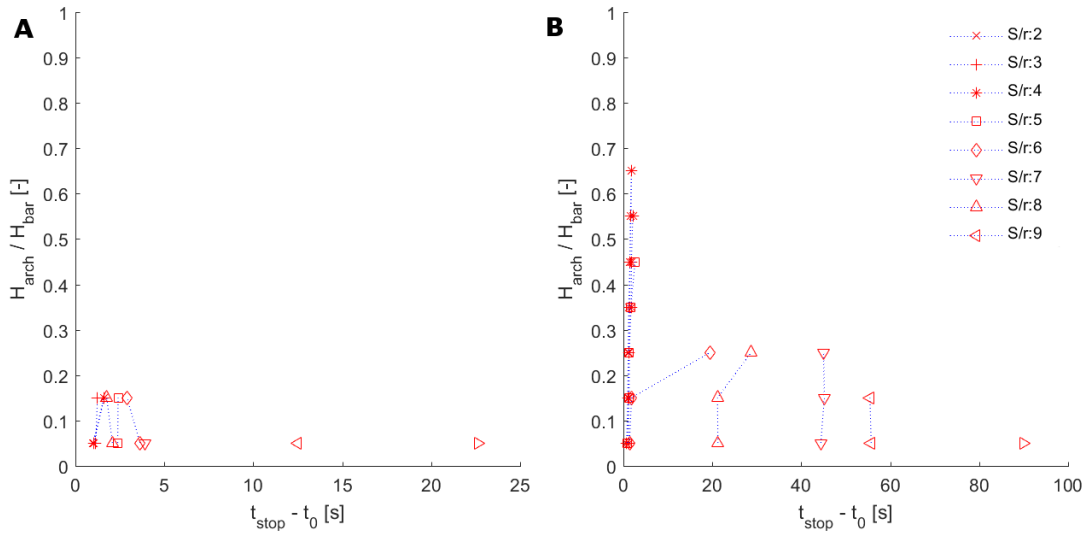
Figure 2: Ratio between the height of the arch and the height of the barrier with respect to the time of arching for $\theta = 10°$ (A) and $\theta = 20°$ (B)

- $\theta = 30°$: frictional forces balance inertial ones. Stable clogging occurs up to $S/r < 9$. For $S/r < 5$ jamming verifies almost instantaneously, and after this value clogging involves only few layers of grains (Fig. 3 (A));

- $\theta = 35°$: inertial forces prevail. Jamming occurs rapidly up to $S/r \leq 4$; for $S/r = 5$ clogging occurs progressively and a a stable configuration is reached at 70 s from the first impact against the barrier. For $S/r > 5$ until $S/r = 9$ clogging involves only one or two layers of grains and verifies later in time (Fig. 3 (B));

- $\theta = 40°$ inertial forces prevail. The same trend as for $\theta = 35°$ is observed. Arching occurs up to $S/r = 8$ (Fig. 3 (C)). This result is in agreement with [12], who stated that for an inclined plane of $40°$ the probability that an arch is destabilized is around 0.3 for $S/D = 5$.
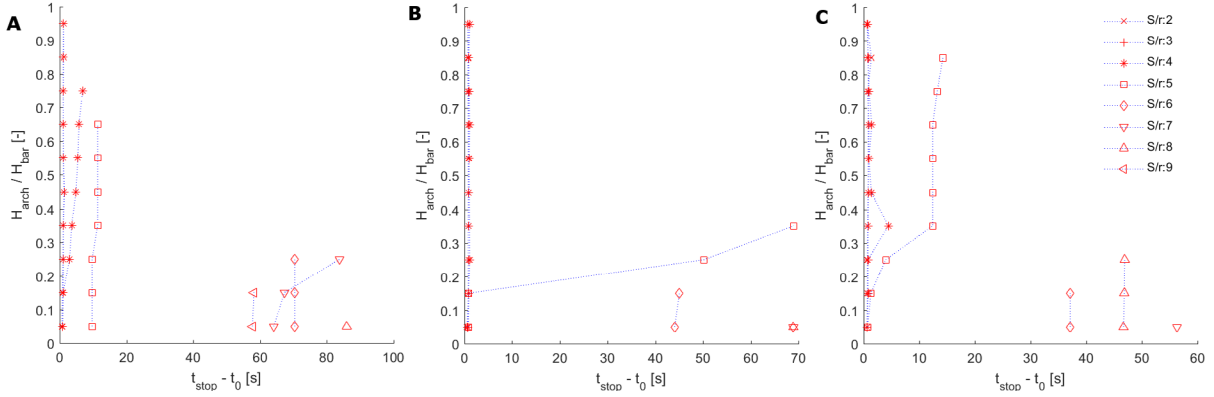
Figure 3: Ratio between the height of the arch and the height of the barrier with respect to the time of arching for $\theta = 30°$ (A), $\theta = 35°$ (B) and $\theta = 40°$ (C)

Fig. 4 shows how the amount of material flowing through the barrier varies with respect to the outlet size. A negligible amount of material passes through the outlet of the barrier for $S/r \leq 4$. Almost the whole material is retained for $\theta = 10°$ independently from the outlet width. A substantial material retainment is observed also for $\theta = 20°$. For $\theta \geq 30°$ an increasing amount of grains flows through the barrier by raising S/r (starting from $S/r = 5$) and a stable configuration is reached with about $90 - 95\%$ of the material fully retained. Concerning the impact forces on the barrier, the results examine the following variables for each outlet size S/r and slope θ: (1) the maximum value of the normal impact force $\mathbf{F}^{N}_{max}$ exerted against the barrier (Fig. 5 (A)), (2) the maximum value of the x torque $\mathbf{M}^{x}_{max}$ exerted to the barrier (Fig. 5 (B)), (3) the ratio between the maximum value of the normal force and the maximum value that would have been registered if the barrier had been completely closed $\mathbf{F}^{N}_{0}$ (Fig. 6 (A)), (4) the ratio between the maximum value of the normal force and its value in static condition $\mathbf{F}^{N}_{st}$ (Fig. 6 (B)), (5) the maximum normal force exerted against the barrier versus the time lag between first arrival and the time at which the maximum force is registered t_{lag} (Fig. 7). Considering Fig. 5 (A), the results collapse on a narrow envelope, with no evidence of a specific trend for varying S/r. A significant increase of the maximum value is registered by increasing slope incline. The same trend occurs for the momentum exchange (Fig. 5 (B)). Fig. 6 (A) shows the influence of the presence of an outlet in the barrier in term of forces exerted to the barrier itself. For $\theta \geq 20°$ an appreciable reduction $(40 - 60\%)$ is observed, almost irrespective of slope incline and outlet size. Only for $\theta = 10°$ no reduction is, as here the maximum value is due to the single-grain impact, which is the same for both open and close barrier. The
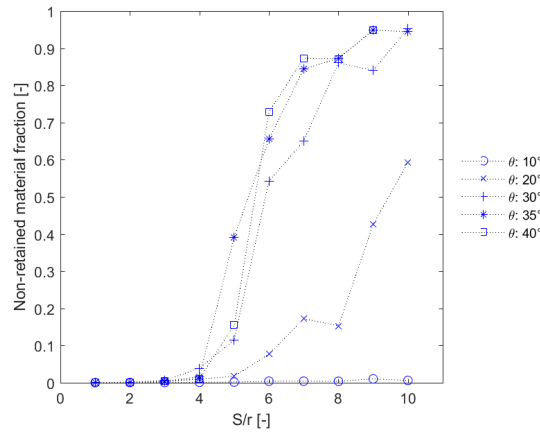
Figure 4: Non retained material fraction with respect to the outlet size of the barrier at complete stop of the discharging mass

plot of Fig. 6(B) highlights that for $S/r \leq 6$ a considerable amount of mass $(75 - 95\%)$ flows through the outlet and thus the static force is far lower the maximum one. Finally, the graph in Fig. 7 shows a considerable scattering of data and a high t_{lag} for $\theta = 20°$. For greater slopes, t_{lag} reduces. For equal slope angle, the data scattering varying the outlet size reduces when increasing the slope angle, with no evident trend considering S/r variation. For $\theta = 10°$ all results converge to the same value, as for all simulations at this slope the maximum value is reached at the same time and corresponds to a single grain impact.

4   DISCUSSION

Results of the simulations allow some preliminary conclusions for what concerns the dynamics of arching and impact against the barrier.

Concerning the arching for a slope angle lower to the internal friction angle $(\theta < \phi_i)$, it is recognized that the steeper the slope is, the higher the arch will be, with jamming occurring more rapidly. Conversely, for $\theta \geq \phi_i$ the steeper the inclined plane is, the less promptly a permanent clogging occurs, and the height of the arch decreases. This might be due to an increase of the flow velocity and thus of the collisional forces which grow at the expense of the frictional ones. Nevertheless, the increment in velocity seems to result in higher arches for lower slopes, as frictional forces still prevail on inertial ones. Here arching originates with progressive clogging (that is the sequence of jamming and unjamming situations until a stable configuration is reached) and lower stable arches form for steepness grater than internal friction angle. This implies that the critical outlet size decreases with increasing slope. It may be inferred that for inertial regimes, in which the collisional dynamics prevails, stable clogging occurs for an outlet size lower or equal to $3 - 4D$. These results are comparable with those found for 3D laboratory experiments
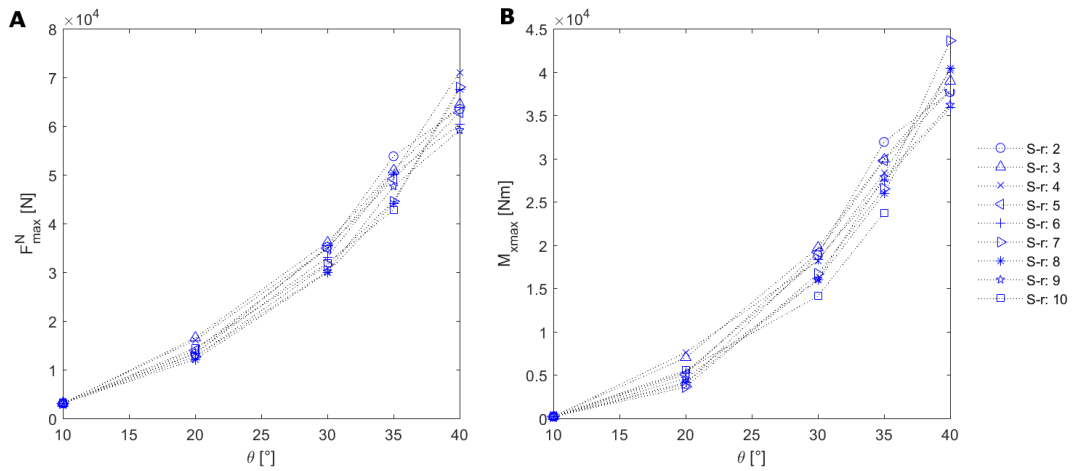
Figure 5: Maximum normal force (A) and maximum momentum in x direction (B) exerted by the discharged mass to the barrier.

on spherical steel beads discharged by a silo: [8] found a critical value $S = 4 - 5D$, while [2] $S = 3D$ and [10] $S = 4D$. Furthermore, for $S/r = 5$ progressive clogging is observed, creating a transitional state of jam and flows, until a stable arch forms. For $6 \leq S/r \leq 9$ arching verifies later in time and therefore stabilizes at a lower height. This tendency suggests that for this setting ore than 80% of the material should flow to allow resisting force to balance driving ones. The increase of slope (and thus velocity) in the collisional regime reduces the clogging time and the flowing of the mass through the outlet. For this reason, the situation for $\theta = 20°$ is equal to $\theta = 40°$, but the amount of retained material and the halt mechanisms are quite different.

The analysis shows that $\mathbf{F}^{\mathrm{N}}_{\mathrm{max}}$ increases by raising θ: velocity grows and the kinetic energy with it, resulting in a greater impact force. Collisions occur more frequently by increasing θ. It seems that this trend is almost independent from the outlet size dimension. For the same reason, the time at which $\mathbf{F}^{\mathrm{N}}_{\mathrm{max}}$ is registered decreases with increasing θ. Referring to Fig. 7, the data scattering for $\theta = 20°$, for which a great gradient among values in time for different outlet is observed, is attributed to great oscillations occurred before reaching a static value, without a specific peak value. It appears that for this inclination motion is considerably decelerated and delayed by frictional forces, preventing the reach of a clear peak value.

5   CONCLUSIONS AND FUTURE PERSPECTIVES

An appropriate modeling of the mechanical process that develops when a granular flow interacts with protection measures is of great concern and a crucial issue. Achieving a deeper understanding of the mechanisms is very important in the perspective of deriving a better structure design. In this context, the present study focuses on open rigid barriers, investigating the arching and the impact dynamics. The research is based on a series
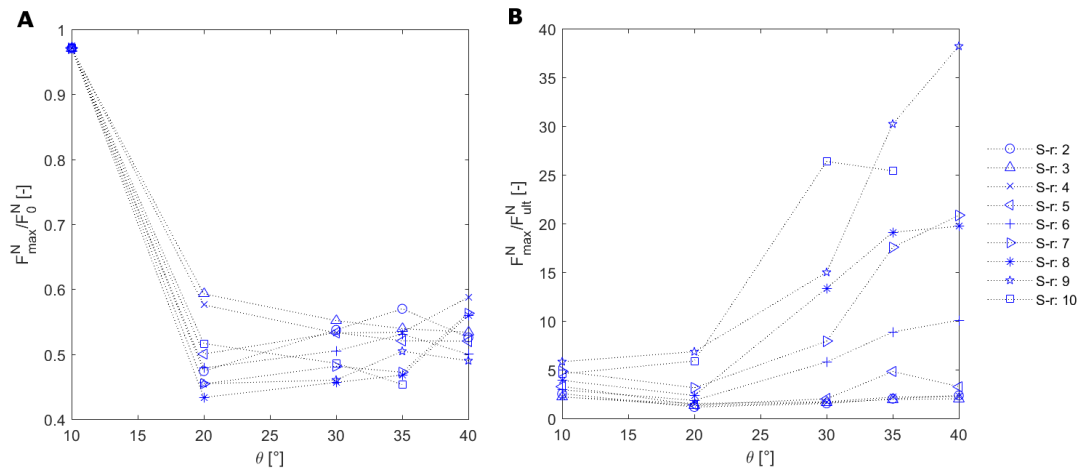
Figure 6: Ratio between maximum value of force for each outlet size and maximum value for a closed barrier with the same slope is plotted in respect to slope angle (A) and ratio between maximum value of the force and its value in static condition for each outlet size in respect to slope angle (B).

of numerical simulations where both outlet size and slope angle are varied in order to separately analyze their influence. The critical discussion of the numerical results has allowed to derive some significant considerations.

The slope incline remarkably affects the prevalent mechanism of motion and thus how arching evolves in time and in height. For a slope lower than the internal friction angle, frictional forces prevail and arching occurs for every outlet size, with a deposit height and clogging time that increase with the slope. For slope angles equal or higher than the internal friction angle, inertial forces prevail and stable arches are observed up to the outlet size $S \leq 3 - 4D$. Furthermore, for $S/r = 5$ a progressive clogging is observed and jamming is no more very rapid. For $6 \leq S/r \leq 8 - 9$ the jamming time increases, with few layers of grains involved in the process. In this configuration the retained mass value is around 5%. This implies that the amount of mass flowing downstream is considerable but the presence of the barrier still provides a significant reduction of kinetic energy. This aspect will be targeted by future works. The trapping efficiency is nevertheless proved for $S/r \leq 5$ for each inclines, with progressive clogging occurring for $S/r = 5$ for slope $\theta \geq \phi_i$. This allows to draw conclusions for what concerns the efficiency and maintenance cost of a barrier. Progressive clogging to some extent prevent a sudden filling of the barrier and thus a quick loss of effectiveness.

The nature of jamming is different if there are two or more adjacent outlet [18]. Stable and/or independent arches cannot form if the width of the racks in the barrier is lower than a certain value. This aspect requires further investigation, which is deferred to future works.
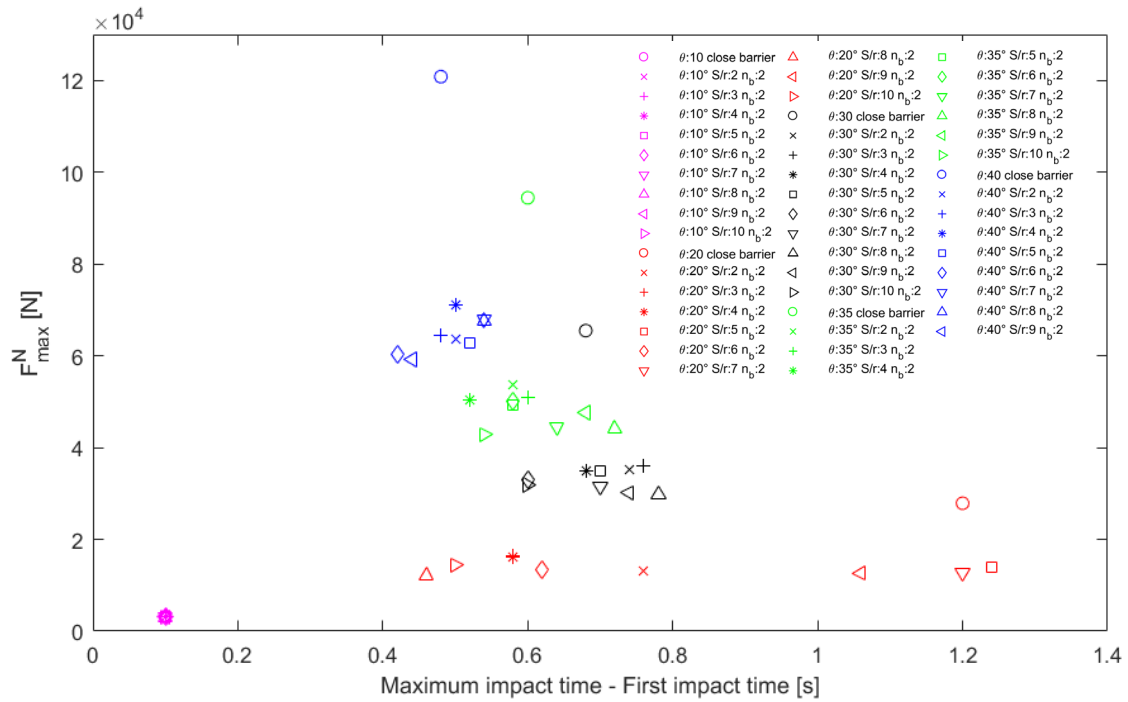
Figure 7: Maximum force exerted against the barrier versus time lag between first arrival and maximum value.

REFERENCES

[1] Albaba, A., Lambert, S.,Nicot, F., Chareyre, B. Relation between microstruscture and loading applied by granular flow to a rigid wall using DEM modeling. *Granular Matter* (2015) **17** (5):603–616.

[2] Pournin, L., Ramaioli, M., Folly, P., Liebling, Th. M. About the influence of friction and polydispersity on the jamming behavior of bead assemblies. *The European Physical Journal E* (2007) **23**:229–235.

[3] Leonardi, A., Wittel, F. K., Mendoza, M., Vetter, R., Herrmann, H. J. Particle-fluid-structure interaction for debris flow impact on flexible barrier. *Computer-Aided Civil and Infrastructure Engineering*, (2015) **31**:323–333.

[4] Hungr, O., Evans, S. G., Bovis, M. J., Hutchinson, J. N. A review of the classification of landslides of the flow type. *Environmental & Engineering Geoscience* (2001) **7** (3):221–238.

[5] Zanuttigh, B. and Lamberti, A. Experimental analysis of the impact of dry avalanches on structures and implication for debris flows. *Journal of Hydraulic Research* (2006) **44** (4):522–534.

[6] Calvetti, F., di Prisco, C., Vairaktaris, E. Impact of dry granular masses on rigid barriers. *IOP Conference Series: Earth and Environmental Science* (2015): doi:10.1088/1755-1315/26/1/012036.

[7] Choi, C. E., Goodwin, G.R., Ng, C. W. W, Cheung,D. K. H., Kwan, J, S. H., Pun, W. K. Coarse granular flow interaction with slit structures *Géotechnique Letters* (2016) **6**:267–274.

[8] Zuriguel, I., Garcimartín, A., Maza, D., Pugnaloni, L. A., Pastor, J. M. Jamming during the discharge of granular matter from a silo. *Physical Review E* (2005) **71**: doi: 10.1103/PhysRevE.71.051303.

[9] Chevoir, F., Gaulard, F., Roussel, N. Flow and jamming of granular mixtures through obstacles. *Europhysics Letters* (2007) **79**: doi: 10.1209/0295-5075/79/14001.

[10] Sheldon, H. G. and Durian, D. J. Granular discharge and clogging for tilted hoppers. *Granular Matter* (2010) **12**:579–585.

[11] Hidalgo, R. C., Lozano, C, Zuriguel, I., Garcimartn, A. Force analysis of clogging arches in a silo. *Granular Matter* (2013): doi: 10.1007/s10035-013-0451-7.

[12] Arvalo, R. and Zuriguel, I. Clogging of granular materials in silos: effect of gravity and outlet size. *Soft Matter* (2016) **12**:123–130.

[13] Magalhães, C. F. M., Moreira, J. G., Atman, A. P. F. Catastrophic regime in the discharge of a granular pile. *Physical Review E - Statistical, Nonlinear, and Soft Matter Physics* (2010) **84**:1–4.

[14] Magalhães, C. F. M., Moreira, J. G., Atman, A. P. F. Segregation in arch formation. *European Physical Journal E* (2012) **35 (5)**. doi 10.1140/epje/i2012-12038-5.

[15] Garcimartín, A., Zuriguel, I., Pugnaloni, L. A., Janda, A. Shape of jamming arches in two-dimensional deposits of granular materials. *Physical Review E - Statistical, Nonlinear, and Soft Matter Physics* (2010) **82**: doi 10.1103/PhysRevE.82.031306

[16] Luding, S. Introduction to discrete element methods: Basic of contact force models and how to perform the micro-macro transition to continuum theory. *European Journal of Environmental and Civil Engineering* (2008): 785–826.

[17] Girolami, L., Hergault, V., Vinay, G., Wachs, A. A three-dimensional discrete-grain model for the simulation of dam-break rectangular collapses: comparison between numerical results and experiments. *Granular Matter* (2012) **14**:381–392.

[18] Mondal, S., Sharma, M. M. Role of flying buttresses in the jamming of granular matter through multiple rectangular outlets. *Granular Matter* (2014) **16**:125–132.